Magnetic Resonance in Medicine 52:927–931 (2004)

Inherent Insensitivity to RF Inhomogeneity in FLASH Imaging

Danli Wang, Keith Heberlein, Stephen LaConte, and Xiaoping Hu*

Radiofrequency (RF) field inhomogeneity is an unavoidable problem in MRI, and it becomes severe at high magnetic fields due to the dependence of B_1 on the sample. It leads to nonuniformities in image intensity and contrast, causing difficulties in quantitative interpretation and image segmentation. In this work, it is observed that with the fast low-angle shot (FLASH) sequence, which is often used for anatomic imaging and morphometric studies, sensitivity to RF inhomogeneity can be substantially reduced when the same coil is used for both transmission and reception, and an appropriate nominal flip angle is employed. This observation can help us understand the signal behavior of FLASH in the presence of RF inhomogeneity, and provide a guide for selecting parameters in FLASH imaging. Magn Reson Med 52:927–931, 2004. © 2004 Wiley-Liss, Inc.

Key words: RF inhomogeneity; FLASH; flip angle; image uniformity; MRI

Because of practical constraints, the radiofrequency (RF) coil used in MRI cannot be built to generate a completely uniform RF field (B_1) or to have a truly uniform reception sensitivity over the field of view (FOV). Nonuniform B_1 leads to a nonuniform flip angle that results in spatial variations in both contrast and intensity, and nonuniformities in reception sensitivity cause image intensity variations. Consequently, RF coil nonuniformities can lead to significant spatial variations in the image contrast and intensity, making quantitative image interpretation and segmentation difficult to achieve. At high magnetic fields, the RF field interacts with the sample significantly, leading to further degradation of the RF uniformity (1). Thus the problem of RF inhomogeneity is exacerbated at high magnetic fields.

A number of investigators have pointed out the importance of correcting B_1 inhomogeneity in tissue segmentation (2–4). Several methods have been developed to rectify this problem (5–10). While these methods have met with good success, they can be computationally intensive, do not account for contrast variations due to nonuniform excitation, and are mostly based on an approximation of the sensitivity field. Recently, an elegant method using spatially varying excitation to compensate for RF inhomogeneity in excitation was introduced for magnetization prepared ultrafast gradient-echo (MPRAGE) imaging, and was demonstrated to be highly effective for 3D MPRAGE imaging (11) even though the compensation was applied only in 2D.

To date, most morphometric studies have been based on high-resolution 3D T_1-weighted images, often acquired with a 3D fast low-angle shot (FLASH) sequence (12) or a 3D MPRAGE sequence (13). While both sequences are widely used, their performance in terms of image uniformity can differ significantly because they are based on different physical principles. With MPRAGE the contrast arises from the preparation of the longitudinal magnetization, and a steady state is not reached during the acquisition of gradient echoes, whereas with FLASH a steady state is reached and the signal intensity is determined from a steady-state equation. With adiabatic inversion, as is commonly used, MPRAGE is monotonically affected by coil sensitivity in both excitation (for the small angles that are usually used (14)) and reception. Its intensity thus increases with coil sensitivity. In contrast, FLASH's dependence on coil sensitivity is not monotonic because of the nonlinear dependence of its signal intensity on the flip angle (see Eq. [1] below). Consequently, for some range of flip angles, the signal's dependence on B_1 is compensated for by the reception sensitivity, if the same coil is used for both transmission and reception, which reduces the sensitivity to coil inhomogeneity. This observation provides a new understanding of the FLASH signal behavior in the presence of B_1 inhomogeneity, and could be beneficial in MRI anatomic studies and facilitate automatic segmentation.

THEORY

Assuming adequate spoiling, and ignoring T_2^* effects and receiver sensitivity, the signal intensity (S) dependence on flip angle (α) and T_1 of a FLASH image (12) is given by

$$S \propto \frac{1 - e^{-TR/T_1}}{1 - \cos(\alpha) \times e^{-TR/T_1}} \times \sin(\alpha). \quad [1]$$

If the same coil that is used for excitation is also used for reception, the signal expression for the image must be modified to include the reception sensitivity of the coil. Assuming that the principle of reciprocity applies (15), the signal expression of a FLASH image is determined by

$$S \propto \frac{1 - e^{-TR/T_1}}{1 - \cos(\kappa \cdot \alpha) \times e^{-TR/T_1}} \times \sin(\kappa \cdot \alpha) \times \kappa. \quad [2]$$

In Eq. [2], κ is a spatially dependent sensitivity factor that modulates both the excitation flip angle and the reception sensitivity, and α is the nominal flip angle. In Eq. [2], we observe that for angles above the Ernst angle, the signal is

Biomedical Imaging Technology Center, Wallace H. Coulter Department of Biomedical Engineering, Emory University/Georgia Institute of Technology, Atlanta, Georgia.

Grant sponsor: NIH; Grant numbers: RO1MH55346; RO1EB00321; Grant sponsors: Georgia Research Alliance; Whitaker Foundation.

*Correspondence to: Xiaoping Hu, Ph.D., Dept. of Biomedical Engineering, 531 Asbury Circle, Suite N305, Atlanta, GA 30322. E-mail: xhu@bme.emory.edu

Received 26 December 2003; revised 6 May 2004; accepted 10 May 2004.

DOI 10.1002/mrm.20217

Published online in Wiley InterScience (www.interscience.wiley.com).

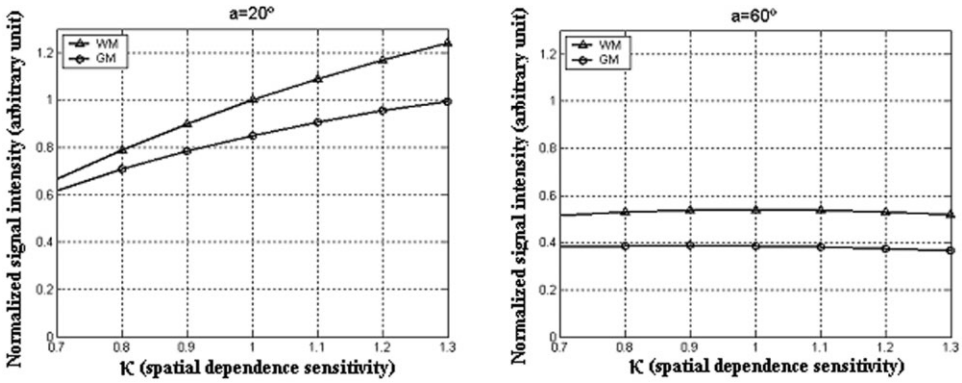

FIG. 1. Simulated FLASH image signal intensity changes with κ in the range of 0.7–1.3 for TR = 45 ms in GM (T_1 = 1286 ms, ρ_0 = 0.69) and WM (T_1 = 788 ms, ρ_0 = 0.61) at 3T. The intensities were normalized by the WM intensity at κ = 1, and nominal flip angle = 20°. The signal intensity changes very slowly when the flip angle is 60°.

approximately inversely proportional to the flip angle, scaled by κ. On the other hand, the receiver sensitivity is proportional to B_1, assuming that the principle of reciprocity (15) holds, and is proportional to κ. Therefore, it is anticipated intuitively that the measured signal, described by Eq. [2], has an approximately constant value over a range of κ for which the flip angle is above the Ernst angle. This approximately constant signal regime can then be used to obtain uniform FLASH images.

To verify the above conjecture, we performed numerical calculations, using Eq. [2], of measured FLASH intensities of white matter (WM) and gray matter (GM) ($T_{1,\ WM}$ = 788 ms, and $T_{1,\ GM}$ = 1286 ms for 3T (16)) as a function of κ for various nominal flip angles, assuming a TR of 45 ms, a typical value for 3D anatomic brain imaging. Normalized proton densities (17) for WM (0.61) and GM (0.69) were also included in the calculation. The intensities were normalized by the WM intensity at κ = 1 and nominal flip angle = 20°. For most imaging setups, the nominal flip angle is the average of the actual flip angle over the sensitive volume of the coil. Therefore, actual flip angles over the FOV center around the nominal angle and κ fluctuates at about one. It is thus important for the region around κ = 1 to be as flat as possible to achieve uniform intensity within the same tissue in the acquired image. Numerical simulations showed that for a small nominal flip angle (< or ~ Ernst angle (GM: 15°, WM: 19° in this case)), the flat region is not around κ = 1, and vice versa. This is illustrated in Fig. 1, where Eq. [2] was evaluated around κ = 1 for the nominal flip angles of 20° and 60°. Signal intensities of WM and GM are not flat around κ = 1 for the flip angle of 20°. In contrast, when the flip angle is 60°, signal intensities are virtually constant. This simulation indicates that when a sufficiently large flip angle is used, the image intensity within the same tissue will be uniform. It is also interesting to note that the difference between the GM and WM (i.e., the image contrast) remains approximately constant in a large range of κ for flip angles greater than the Ernst angle.

MATERIALS AND METHODS

We performed experiments to confirm the above numerical prediction. A Siemens 3 Tesla system equipped with a Sonata gradient set capable of 40 mT/m with a maximum rise time of 200 μs was used for this study. A head coil was used for data acquisition. Since imperfect slice profiles associated with selective excitation pulses may introduce a modulation of α across the slice, complicating Eq. [2], a nonselective excitation pulse was used in conjunction with a 3D-FLASH sequence for simplicity. Experimental data were first collected on a spherical phantom (T_1 = 1240 ms at 3T) with a TR of 45 ms, a TE of 2.61 ms, an FOV of 238 mm × 208 mm × 202 mm, a matrix of 128 × 112 × 96, and nominal flip angles of 10°, 20°, 30°, 40°, 50°, 60°, 70°, and 80°. In addition to the phantom experiment, we also performed an in vivo study on three healthy volunteers, with IRB approval and informed consent, to verify the validity of our theoretical prediction in vivo. In this case, the 3D-FLASH sequence parameters consisted of a TR of 45 ms, a TE of 2.70 ms, an FOV of 200 mm × 200 mm × 166 mm, a matrix of 128 × 128 × 104, and nominal flip angles of 15°, 30°, 45°, 60°, 75°, and 85°.

We processed the resultant data using routines implemented in IDL (Research Systems Inc.). To make a simple quantitative comparison of the dependence on flip angle, we analyzed a single slice from the 3D data set. A central slice in the axial direction was used for the analysis of the phantom images. A profile of the image (along the line indicated in Fig. 2) was examined. In addition, a region of interest (ROI) encompassing the phantom in the image was created and used to calculate the range of intensity over the phantom for each nominal flip angle. Similarly, an axial slice from the human data was analyzed. Profiles of the image along a line (indicated in Fig. 3) that resided in the WM were quantitatively analyzed for each angle. Because the profile from the human images was fairly noisy, the profiles were fitted to a second-order polynomial curve before the intensity range of the fitted profiles was calculated to ascertain the spatial variation.

RESULTS AND DISCUSSION

Figure 2 shows images of the uniform phantom acquired at two different flip angles (20° and 50°, respectively). Spatial variation in the image obtained with a 20° flip angle (Fig. 2a) is severe (the center of the image is much brighter than the surrounding areas). The normalized intensity range (the maximum intensity in the image minus the minimum, divided by the maximum) for this image is 0.63. In contrast, when a 50° nominal flip angle was used, the variation decreased to a negligible level (Fig. 2b) and the normalized

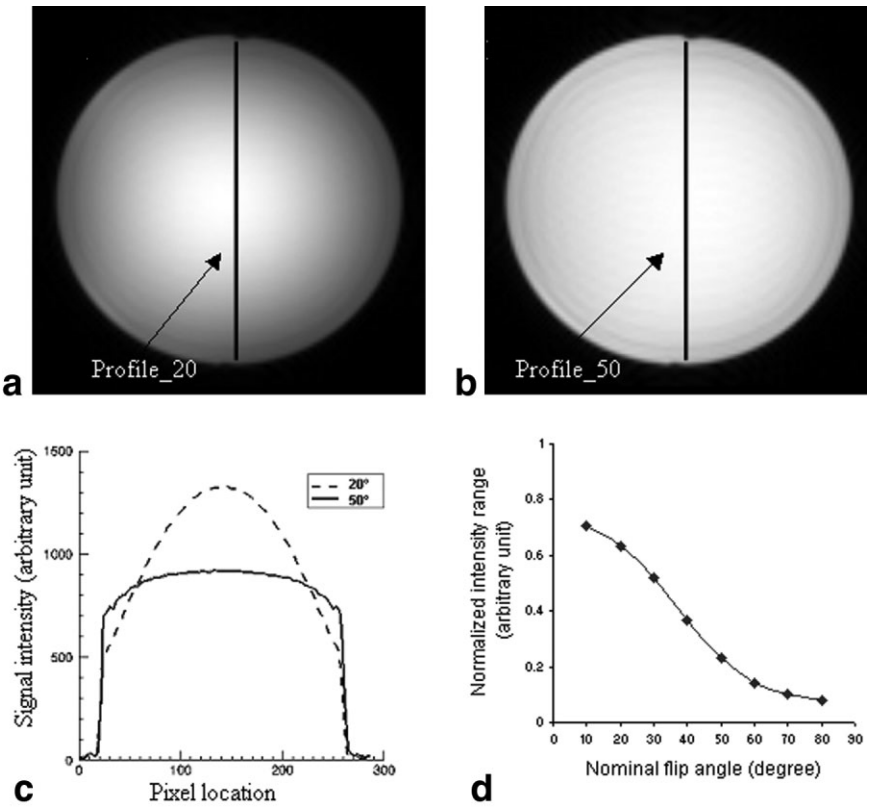

FIG. 2. A 2D image and intensity profiles obtained from a 3D-FLASH image of the phantom at flip angle = 20° (**a**) and 50° (**b**). The intensity variation in the phantom image decreased with flip angle, as shown in the vertical profiles in **c**. **d:** The normalized intensity range varies with the nominal flip angle.

intensity range dropped to 0.23. This dependence of image uniformity on the nominal flip angle can also be observed in the image profiles, shown in Fig. 2c, wherein the 50° profile (solid line) is approximately flat while the 20° profile (dashed line) exhibits substantial variation. The normalized intensity range of the phantom image is plotted against the nominal flip angle in Fig. 2d, illustrating that the relative intensity variation in the phantom image decreases with α. This result, in agreement with the theoretical analysis given above, suggests that a nominal angle of 40–60° would be a good choice for image uniformity.

The results from the human study are illustrated in Fig. 3. Similarly to the phantom data, the image of the smallest flip angle used (15°) exhibits the largest spatial variation (i.e., the center is brighter than the outer regions). This spatial variation is diminished when larger flip angles are used. As an example of the reduced intensity variation, profiles along the black line (Fig. 3a) in images obtained at 15° and 45° are plotted in Fig. 3b. In this plot, the profile of the 15° image (solid line) exhibits substantial variation, while that of the 45° image (dashed line) is essentially flat. The normalized intensity range (maximum value of the fitted profile minus the minimum value of the fitted profile, divided by the maximum fitted value) was calculated from each profile and plotted against the nominal flip angle in Fig. 3c. This result exhibits good correspondence with the phantom results in Fig. 2d. At a nominal flip angle of 15°, the signal intensity range is much larger than that at other angles. When the flip angle was increased to 45°, 60°, and 75°, the intensity ranges dropped to about less than half of that at 15°. A broad shoulder with a gradual decrease is seen between 40° and 75°. This result qualitatively parallels the phantom result and demonstrates that insensitivity to RF inhomogeneity can be achieved if a sufficiently large flip angle is used during the data acquisition. Of course, the exact angle at which this insensitivity is optimal depends on the TR, the T_1 of the tissue of interest, and the spatial distribution of the RF field.

In Fig. 4, we present data demonstrating the dependence of signal (or signal-to-noise ratio (SNR), as the noise is constant) and contrast on the flip angle. Specifically, the measured signal in WM (the GM signal shows a similar trend, but to avoid cluttering the figure, it was not included) is plotted vs. flip angle and compared with numerical calculations. Undoubtedly, there is a significant reduction in signal (and SNR) with increasing flip angles because the angles used were mostly above the Ernst angle. While the overall SNR is an important measure of image quality, a more important measure is the contrast (or, equivalently, the contrast-to-noise ratio (CNR), as the noise level remains the same). Therefore, Fig. 4 also provides a comparison of numerically-derived WM vs. GM contrast as a function of flip angle with the experimentally obtained values. A good agreement between the simulation and the experiment is evident in Fig. 4. Although the contrast is also reduced at large flip angles, it peaks at an angle larger than the Ernst angle (30° instead of 15°) and decreases more slowly for large flip angles. Since going beyond 60° leads to only a small improvement in uniformity (see Fig. 3c), but a substantial reduction in contrast, it is recommended that a flip angle of 40–55° be used when other imaging parameters are the same, as done in this experiment. While we present results only for a TR of

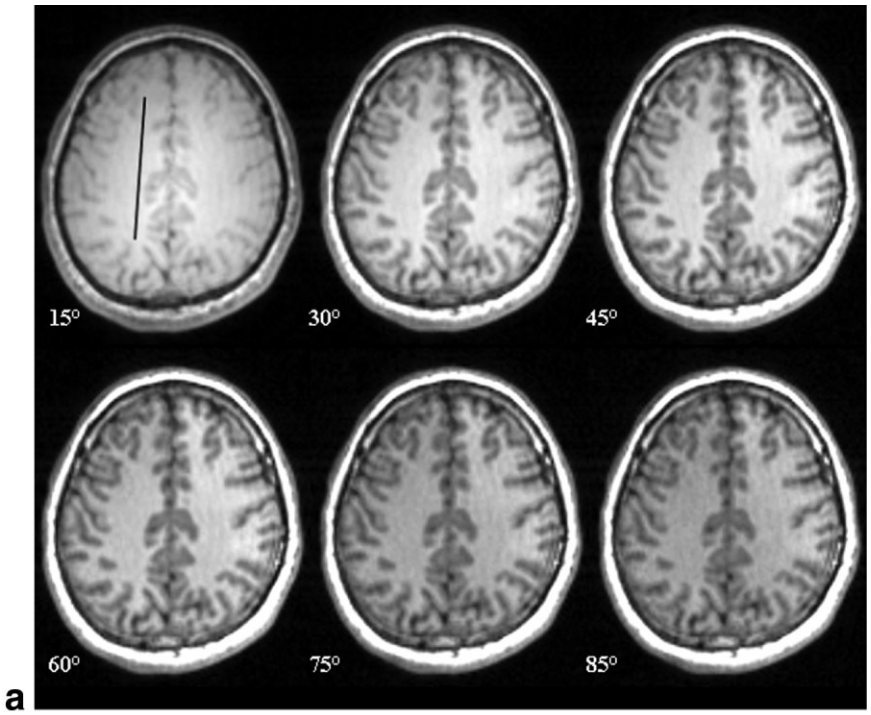

FIG. 3. FLASH images of a volunteer acquired at flip angles of 15°, 30°, 45°, 60°, 75°, and 85°. An increase in image uniformity is seen with increasing flip angle. A line in the WM, shown in the first image, indicates the location of the spatial profile. **b:** Spatial profiles in images obtained with flip angles of 20° and 50°, respectively. **c:** Fitted image profile range vs. nominal flip angle.

45 ms, a shorter TR would not alter the general observation reported here (i.e., above the Ernst angle, FLASH images should be relatively insensitive to coil sensitivity).

It should be noted that the validity of Eq. [2] depends on two things: the validity of Eq. [1], which relies on complete spoiling of the transverse magnetization and the validity of reciprocity. The latter can be violated at high magnetic fields (15). This factor may be already present in our human data at 3 Telsa, although it is not very severe. However, for higher magnetic fields, the validity of the current results may be degraded.

Undoubtedly, the flat signal region can only be of a finite extent. Therefore, the insensitivity of FLASH to RF inhomogeneity is only valid for a limited range of variations that arise in relatively uniform coils, and probably is not valid over the entire sensitivity range of a surface coil.

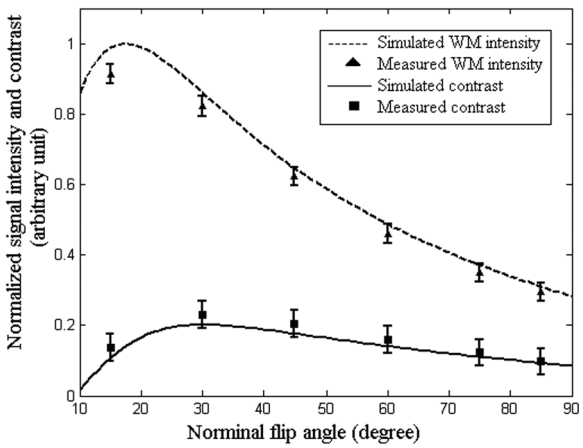

FIG. 4. Simulated contrast and measured contrast of FLASH image as a function of nominal flip angles with TR = 45 ms in GM (T_1 = 1286 ms) and WM (T_1 = 788 ms) at 3T. The simulated contrast assumed a κ of 1.10. The measured signal in WM is also plotted vs. nominal flip angle, and compared with numerical calculations.

CONCLUSIONS

Based on theoretical arguments and experimental data, we have demonstrated that the FLASH sequence can have

reduced sensitivity to RF inhomogeneity if a single coil is used for both transmission and reception, and an appropriate nominal flip angle is used. Under this condition, variations due to receiver sensitivity offset the variations due to transmitter nonuniformities, thereby eliminating the deleterious effect of RF inhomogeneity in the image data. The observations made in this FLASH imaging study suggest a simple way to minimize the effects of B_1 inhomogeneity, and should be of benefit for investigators choosing FLASH sequence parameters for use in anatomic studies.

ACKNOWLEDGMENTS

The authors thank Drs. Scott Peltier and Yasser Kadah for helpful discussions.

REFERENCES

1. Collins CM, Li S, Smith MB. SAR and B_1 field distributions in a heterogeneous human head model within a birdcage coil. Magn Reson Med 1998;40:847–856.
2. Simmons SR, Arridge GJ, Barker GJ, Williams SC. Sources of intensity nonuniformity in spin echo images at 1.5 T. Magn Reson Med 1994;32: 121–128.
3. Lim KO, Pfefferbaum A. Segmentation of MR brain images into cerebrospinal fluid spaces, white and gray matter. J Comput Assist Tomogr 1989;13:588–593.
4. Narayana PA, Borthakur A. Effect of radiofrequency inhomogeneity correction on the reproducibility of intra-cranial volumes using MR image data. Magn Reson Med 1995;33:396–400.
5. Andersen AH, Zhang Z, Avison MJ, Gash DM. Automated segmentation of multispectral brain MR images. J Neurosci Methods 2002;122:13–23.
6. Clare S, Alecci M, Jezzard P. Compensating for B_1 inhomogeneity using active transmit power modulation. Magn Reson Imaging 2001;19:1349–1352.
7. Zhou LQ, Zhu YM, Bergot C, Laval-Jeantet AM, Bousson V, Laredo JD, Laval-Jeantet M. A method of radio-frequency inhomogeneity correction for brain tissue segmentation in MRI. Comput Med Imaging Graph 2001;25:379–389.
8. Koivula A, Alakuijala J, Tervonen O. Image feature based automatic correction of low-frequency spatial intensity variations in MR images. Magn Reson Imaging 1997;15:1167–1175.
9. Ugurbil K, Garwood M, Rath AR, Bendall MR. Amplitude-modulated and frequency phase-modulated refocusing pulses that induce plane rotations even in the presence of inhomogeneous B_1 fields. J Magn Reson 1988;78:472–497.
10. Talagala SL, Gillen J. Experimental determination of 3-dimensional RF magnetic-field distribution of NMR coils. J Magn Reson 1991;94:493–500.
11. Deichmann R, Good CD, Turner R. RF inhomogeneity compensation in structural brain imaging. Magn Reson Med 2002;47:398–402.
12. Haase A, Frahm J, Matthaei D, Hanicke W, Merboldt KD. FLASH imaging—rapid NMR imaging using low flip-angle pulses. J Magn Reson 1986;67:258–266.
13. Mugler JP, Brookeman JR. 3-Dimensional magnetization-prepared rapid gradient-echo imaging (3D MP-RAGE). Magn Reson Med 1990; 15:152–157.
14. Blüml S, Schad LR, Stepanow B, Lorenz WJ. Spin-lattice relaxation time measurement by means of a TurboFLASH technique. Magn Reson Med 1993;30:289–295.
15. Hoult DI. The principle of reciprocity in signal strength calculations—a mathematical guide. Concepts Magn Reson 2000;12:173–187.
16. Wansapura JP, Holland SK, Dunn RS, Ball WS. NMR relaxation times in the human brain at 3.0 tesla. J Magn Reson 1999;9:531–538.
17. Szumowski J, Simon JH. Fat and water signal separation methods. In: Stark DD, Bradley WG, editors. Magnetic resonance imaging. 3rd ed. St. Louis: Mosby; 1999. p 162.